Zinc-Iron Bimetallic MOF-Integrated Thermosensitive Hydrogel for Breast Cancer Immunotherapy *via* Ferroptosis-Induced cGAS–STING Activation

Yihao Zhan, Xiangyan Chen*, and Yantao Li*

Qingdao Key Laboratory of Biomacromolecular Drug Discovery and Development, State Key Laboratory Base of Eco-Chemical Engineering, College of Chemical Engineering, Qingdao University of Science and Technology, Qingdao 266042, China

Abstract. Breast cancer is characterized by a profoundly immunosuppressive tumor microenvironment (TME), which severely limits therapeutic efficacy and immune activation. Here, we develop a zinc-iron bimetallic MOF-integrated thermosensitive hydrogel (ZF-Gel) for in situ breast cancer immunotherapy *via* ferroptosis-induced cGAS-STING activation. Upon intratumoral injection, ZF-Gel undergoes rapid temperature-triggered sol-gel transition, forming a stable intratumoral depot that enables sustained local retention. Mechanistically, the Zn/Fe bimetallic MOF induces oxidative stress and lipid peroxidation, triggering ferroptosis. Ferroptosis-associated damage signals, together with Zn^{2+}-mediated regulation, activate the cGAS–STING pathway, leading to IRF3 phosphorylation and downstream immune gene expression, thereby coupling tumor cell death with innate immune sensing and adaptive immune activation. *In vitro*, ZF-Gel exhibits pronounced antiproliferative effects against breast cancer cells. This work establishes a mechanism-driven hydrogel-MOF platform that integrates local retention, regulated cell death, and innate–adaptive immune crosstalk, offering a promising strategy for immunologically cold breast tumors.

1 Introduction

Breast cancer remains one of the most prevalent malignancies among women worldwide and continues to pose a significant threat to public health[1]. Despite advances in surgery, radiotherapy, chemotherapy, and targeted therapy, clinical outcomes remain suboptimal, particularly for triple-negative breast cancer (TNBC), owing to pronounced tumor heterogeneity and therapeutic resistance[2]. In recent years, immune checkpoint inhibitors (ICIs) have demonstrated remarkable success in several solid tumors[3]. However, breast cancer is typically characterized by an immunologically "cold" tumor microenvironment (TME), marked by limited immune cell infiltration and dominant immunosuppressive signaling, which results in poor responsiveness to immunotherapy[4]. Therefore, strategies capable of effectively reprogramming the TME and activating antitumor immunity are urgently needed.

Ferroptosis, an iron-dependent form of regulated cell death driven by lipid peroxidation, has emerged as a promising therapeutic modality for cancer treatment[5]. Beyond direct tumor cell elimination, ferroptosis can induce immunogenic cell death (ICD) by releasing damage-associated molecular patterns (DAMPs) and tumor-associated antigens, thereby promoting dendritic cell maturation and T-cell activation[6]. Mechanistically, intracellular iron accumulation and glutathione peroxidase 4 (GPX4) inactivation sensitize tumor cells to ferroptosis, while Fenton reaction-mediated hydroxyl radical (·OH) generation represents a key chemical driver of lipid peroxidation[7]. Accordingly, introducing exogenous iron sources to amplify intratumoral Fenton reactions has become an effective strategy for ferroptosis induction[8]. In parallel, the cyclic GMP-AMP synthase-stimulator of interferon genes (cGAS-STING) pathway functions as a central innate immune sensing axis that detects cytosolic DNA and initiates type I interferon (IFN-I)-mediated immune responses[9]. Emerging evidence suggests that ferroptosis-associated mitochondrial damage and DNA leakage can activate cGAS, leading to downstream STING-TBK1-IRF3 signaling and amplification of antitumor immunity[10]. This establishes a mechanistic linkage between ferroptosis and innate-adaptive immune crosstalk. Notably, Zn^{2+} has been identified as a key modulator of cGAS-STING signaling, and its regulatory role is mainly achieved through two interconnected mechanisms: on one hand, Zn^{2+} can perturb mitochondrial membrane integrity, thereby enhancing mitochondrial ROS generation and further promoting the release of mitochondrial DNA into the cytoplasm-an essential step for cGAS activation; on the other hand, Zn^{2+}-mediated ROS amplification can directly stabilize the binding of cGAS to cytosolic DNA, accelerating the catalytic activity of cGAS and amplifying the downstream

* Corresponding author: cxy@qust.edu.cn (Xiangyan Chen), liyantao@qust.edu.cn (Yantao Li).

STING-TBK1-IRF3 signaling cascade[11]. This specific regulatory mechanism of Zn^{2+} provides a solid theoretical basis for bimetallic synergy (Fe^{3+}/Zn^{2+}) in ferroptosis-driven immunotherapy.

Metal-organic frameworks (MOFs) have attracted increasing attention in nanomedicine owing to their tunable structures, high loading capacity, and stimulus-responsive degradation within the TME[12]. In particular, bimetallic MOFs enable the integration of multiple metal-mediated functions, including catalytic activity and immune modulation[13]. However, rapid systemic clearance and insufficient tumor retention of nanomaterials remain major challenges that limit their therapeutic efficacy[14]. Thermosensitive hydrogels, especially Pluronic F127-based systems, undergo temperature-triggered sol–gel transition, allowing minimally invasive injection and in situ formation of stable depots for sustained release[15]. Such systems provide an effective approach to prolong local retention, reduce systemic toxicity, and maintain a persistent therapeutic microenvironment. Despite these advances, the rational integration of ferroptosis-inducing catalytic components with immune-activating signaling pathways within a locally retained delivery system remains insufficiently explored. More importantly, how to simultaneously achieve efficient intratumoral retention, amplified ferroptosis induction, and robust cGAS–STING activation remains a key unresolved challenge for immunologically cold breast tumors.

Herein, we developed a zinc-iron bimetallic MOF-integrated thermosensitive hydrogel (ZF-Gel) to achieve in situ breast cancer immunotherapy via ferroptosis-induced cGAS-STING activation. Upon intratumoral injection, ZF-Gel undergoes rapid temperature-triggered gelation, forming a stable depot for prolonged local retention. The Fe^{3+}-mediated Fenton reaction induces ROS accumulation and lipid peroxidation, thereby triggering ferroptosis, while ferroptosis-associated signals, together with Zn^{2+} regulation, activate the cGAS-STING pathway to amplify antitumor immune responses. This platform integrates localized catalytic therapy with immune activation, enabling synergistic regulation of tumor cell death and immune responses. This study systematically investigates the physicochemical properties, *in vitro* antitumor efficacy, and immune activation mechanisms of ZF-Gel, providing a promising strategy for the treatment of immunologically cold breast cancer.

2 Materials and methods

2.1 Materials

Iron acetylacetonate, 2-methylimidazole (2-MeIM), zinc nitrate hexahydrate, and Pluronic F127 (Poloxamer 407) were used as received without further purification.

2.2 Synthesis of ZF-Gel

Zn-Fe bimetallic MOF nanoparticles (ZF NPs) were prepared *via* a one-pot method. Briefly, 140 mg of zinc nitrate hexahydrate and 60 mg of iron acetylacetonate were dissolved in 2 mL of methanol to form the metal precursor solution, while 340 mg of 2-methylimidazole was dissolved in 4 mL of deionized water as the ligand solution. Under continuous stirring at 30°C in a sealed vessel, the metal precursor solution was added dropwise into the ligand solution and allowed to react for 12 h. The resulting precipitate was collected by centrifugation (6000 rpm, 10 min), washed with a mixture of methanol and deionized water, and finally redispersed in deionized water.

For hydrogel fabrication, 1,200 mg of Pluronic F127 was dissolved in 8 mL of the ZF NPs dispersion at 10°C, followed by degassing for 2 h to remove air bubbles. The obtained solution was then transferred into molds and incubated at 37°C for approximately 3 min, during which F127 underwent a temperature-triggered sol–gel transition, forming a stable three-dimensional hydrogel network with uniformly encapsulated ZF NPs.

Preparation method of pure F127 hydrogel: Dissolve 1200 mg of PranPluronic F127 in 8 mL of deionized water, stir at 10°C until complete dissolution, then degas for 2 hours to remove bubbles. Transfer the resulting solution to a mold and incubate at 37°C for approximately 3 minutes to induce sol-gel transition, forming pure F127 hydrogel.

2.3 Cell lines and culture

Murine breast cancer 4T1 cells and HUVECs were obtained from the National Infrastructure of Cell Line Resource (China) and cultured in RPMI 1640 supplemented with 10% FBS and 1% penicillin–streptomycin at 37°C with 5% CO_2. All experiments were performed using cells in the logarithmic growth phase, seeded at a density of approximately 5×10^3 cells per well in 96-well plates and allowed to adhere overnight before further treatment.

For in vitro cytotoxicity assessment, the MTT assay was employed to evaluate the effects of PBS, F-Gel, and ZF-Gel at various concentrations (1-16 $mg \cdot mL^{-1}$) on cell viability after 24 h of treatment, thereby determining the concentration-dependent toxicity profile of each material. Intracellular reactive oxygen species (ROS) levels in 4T1 cells were measured using the DCFH-DA fluorescent probe after treatment with hydrogels at 8 $mg \cdot mL^{-1}$ for 12 h, assessing the oxidative stress induced by the materials. Additionally, the killing effect on 4T1 cells was visualized by Calcein AM/PI double staining following treatment with hydrogels at 8 $mg \cdot mL^{-1}$ for 24 h. All experiments were independently repeated three times, and results were expressed as mean ± standard deviation with statistical analysis performed.

3 Results and discussion

3.1 Synthesis and characterization of ZF NPs

The morphology and structural features of ZF NPs were systematically characterized by scanning electron microscopy (SEM) and transmission electron

microscopy (TEM). As illustrated in Fig. 1a, SEM images revealed that ZF NPs exhibited a uniform polyhedral morphology with smooth surfaces and good mono-dispersity, indicative of well-controlled nucleation and growth during the one-pot synthesis process. TEM analysis (Fig. 1b) further confirmed the distinct dodecahedral crystalline architecture of individual nanoparticles, consistent with the characteristic dodecahedral geometry inherent to zeolitic imidazolate framework (ZIF)-type MOF structures. These results verify the successful formation of a well-ordered crystalline coordination network between the bimetallic centers (Zn^{2+}/Fe^{3+}) and 2-MeIM ligands.

Statistical analysis of TEM images showed that ZF NPs possessed an average diameter of 129.46 ± 0.14 nm with a narrow and symmetric Gaussian size distribution (Fig. 1c), demonstrating high batch-to-batch reproducibility and exceptional size uniformity. Such nanoscale dimensions are favorable for intratumoral retention and efficient cellular internalization.

To verify the elemental composition and spatial distribution of the bimetallic constituents, high-angle annular dark-field scanning transmission electron microscopy (HAADF-STEM) coupled with energy-dispersive X-ray spectroscopy (EDS) elemental mapping was performed (Fig. 1d). The resulting elemental maps demonstrated homogeneous and spatially coincident co-distribution of carbon (C), oxygen (O), zinc (Zn), and iron (Fe) signals throughout the entire nanoparticle volume, with no discernible phase segregation or elemental aggregation. This uniform elemental distribution unambiguously confirms the successful co-coordination of both Zn^{2+} and Fe^{3+} within a single MOF lattice, rather than the formation of discrete monometallic phases. The close spatial integration of Zn and Fe provides a structural basis for synergistic catalytic activity and immune modulation in the tumor microenvironment.

Taken together, these comprehensive characterization results demonstrate that ZF NPs possess well-defined morphology, uniform nanoscale size, and homogeneous bimetallic distribution, providing a robust structural foundation for subsequent hydrogel integration and therapeutic applications.

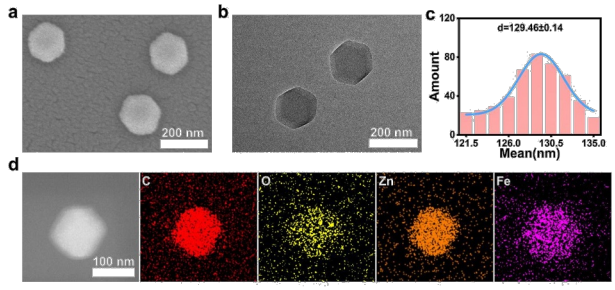

Figure 1. Synthesis and characterization of Zn-Fe bimetallic MOF nanoparticles (ZF NPs). (a) SEM image of ZF NPs. (b) TEM image of ZF NPs. (c) Particle size distribution of ZF NPs. (d) HAADF-STEM image and corresponding EDS elemental mapping of C, O, Zn, and Fe in ZF NPs.

3.2 Microstructural and rheological characterization of ZF-Gel

The physicochemical properties of ZF-Gel were systematically evaluated by scanning electron microscopy (SEM), oscillatory rheology, and *in vivo* fluorescence imaging.

SEM analysis of lyophilized samples revealed that pure F127 hydrogel (F-Gel) possessed a well-defined three-dimensional interconnected porous network, characterized by uniformly distributed pores, smooth and continuous pore walls, and a structurally intact skeletal framework (Fig. 2a), confirming the capacity of F127 to self-assemble into a stable porous scaffold under aqueous conditions. After incorporation of ZF NPs, ZF-Gel (Fig. 2b) retained the overall porous architecture while displaying nanoparticle deposition along the pore walls, indicating successful encapsulation and homogeneous distribution of ZF NPs within the hydrogel matrix. The interconnected microporous structure is expected to facilitate mass transport and support sustained release behavior.

The viscoelastic properties of ZF-Gel were further assessed by oscillatory rheological measurements (Fig. 2c). Within the linear viscoelastic region at low strain amplitudes, the storage modulus (G′) consistently exceeded the loss modulus (G″), with G′ maintained at approximately 10^3 Pa, indicating dominant elastic behavior and good structural integrity. With increasing strain, both moduli gradually decreased, and a crossover point (G′ = G″) was observed at higher strain, reflecting network disruption and a transition to viscous behavior. This typical shear-thinning characteristic suggests that ZF-Gel can be readily injected under shear stress and rapidly recover its gel state in situ, demonstrating favorable injectability and gelation performance.

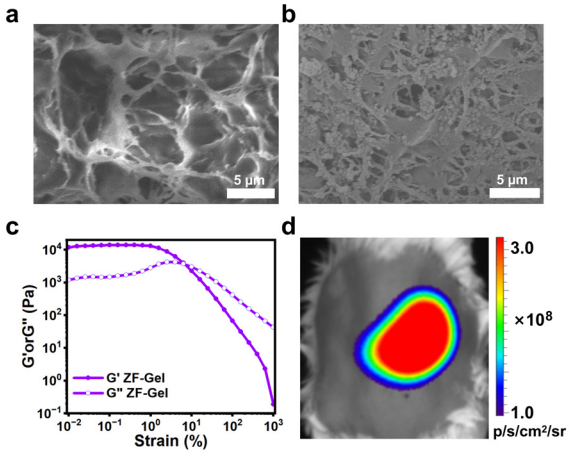

Figure 2. Microstructure, rheological properties and intratumoral retention of ZF-Gel. (a) SEM image of pure F127 hydrogel (F-Gel). (b) SEM image of ZF-Gel. (c) Storage modulus (G′) and loss modulus (G″) of ZF-Gel as a function of strain amplitude. (d) *In vivo* fluorescence imaging of intratumoral retention of ZF-Gel.

The intratumoral retention performance of ZF-Gel was further validated by *in vivo* fluorescence imaging following intratumoral administration of fluorescently

labeled formulations (Fig. 2d). Strong, spatially confined fluorescence signals were detected at the tumor site, with a radiant efficiency of 3.0×10^8 p/s/cm^2/sr. The fluorescence distribution closely matched the tumor region with minimal signal diffusion, indicating rapid in situ gelation and formation of a stable intratumoral depot. This localized retention effectively reduces systemic dispersion and enables prolonged retention of therapeutic components within the tumor microenvironment.

Overall, ZF-Gel exhibits a well-defined porous structure, favorable mechanical properties, excellent injectability, and effective intratumoral retention, providing a solid physicochemical basis for its subsequent therapeutic performance.

3.3 Biosafety evaluation and selective antitumor activity of ZF-Gel

To assess the biocompatibility and tumor-selective cytotoxicity of ZF-Gel, cell viability assays were conducted on human umbilical vein endothelial cells (HUVECs) and murine 4T1 breast cancer cells over a concentration range of 1-16 mg mL^{-1}. As shown in Fig. 3a, both F-Gel and ZF-Gel maintained HUVEC viability above 85% at all tested concentrations, with no significant difference compared to the negative control (P> 0.05). These results confirm that neither the Pluronic F127 hydrogel matrix nor the encapsulated ZF nanoparticles (NPs) elicit appreciable cytotoxicity toward normal vascular endothelial cells, establishing the favorable biocompatibility of the ZF-Gel system and supporting its suitability for *in vivo* administration.

In contrast, ZF-Gel exhibited pronounced, concentration-dependent cytotoxicity against 4T1 cells (Fig. 3b). Whereas the NC and F-Gel groups maintained high viability across all concentrations, ZF-Gel treatment induced a progressive reduction in 4T1 cell viability with increasing dose, with substantial cytotoxic effects becoming evident at 8 and 16 mg mL^{-1}. This selective antiproliferative activity against tumor cells, in the absence of significant toxicity toward normal cells, is attributable to the tumor microenvironment (TME)-responsive behavior of ZF-Gel. Notably, MOF materials are well-documented to exhibit pH-dependent structural stability: their coordination bonds are prone to cleavage under the mildly acidic conditions (pH 5.5-6.5) of the TME, which is significantly lower than the physiological pH (7.4) of normal tissues, thereby triggering framework degradation and localized release of Fe^{3+} and Zn^{2+} ions. Furthermore, the zinc-iron bimetallic MOF in ZF-Gel demonstrates superior degradation kinetics under acidic conditions compared to single-metal Fe-based or Zn-based MOFs, as the synergistic interaction between Fe^{3+} and Zn^{2+} weakens the coordination network, accelerating both framework breakdown and the targeted release of metal ions within the tumor site. This TME-responsive structural instability and enhanced degradation efficiency of the bimetallic MOF are key to concentrating cytotoxic activity within tumors while sparing surrounding healthy tissue.

To visually corroborate these findings, calcein-AM/propidium iodide (PI) live/dead co-staining was performed (Fig. 3c). Cells in the NC and F-Gel groups displayed predominantly green fluorescence (live cells) with negligible red signal (dead cells), consistent with the quantitative viability data. In striking contrast, ZF-Gel-treated 4T1 cells exhibited a near-complete shift to red fluorescence, indicative of extensive cell death. Notably, the diffuse, rounded morphology of the dead cells - rather than the membrane-blebbing pattern characteristic of apoptosis - is morphologically consistent with ferroptotic cell death, providing preliminary evidence in support of the proposed mechanism of action.

To directly evaluate intracellular oxidative stress and lipid peroxidation, a hallmark biochemical feature of ferroptosis, fluorescence imaging using a lipid peroxidation-sensitive probe was performed (Fig. 3d). Both the NC and F-Gel groups exhibited negligible fluorescence, reflecting basal oxidative levels under physiological conditions. In contrast, ZF-Gel-treated 4T1 cells displayed intense, diffuse green fluorescence, indicative of markedly elevated intracellular lipid peroxidation. This observation is mechanistically consistent with Fe^{3+}-catalyzed Fenton-type reactions generating hydroxyl radicals (·OH) that initiate lipid peroxidation cascades, further amplified by Zn^{2+}-mediated mitochondrial dysfunction and reactive oxygen species (ROS) accumulation. The resulting oxidative burden overwhelms cellular antioxidant defenses and drives ferroptotic cell death by enhancing lipid peroxidation.

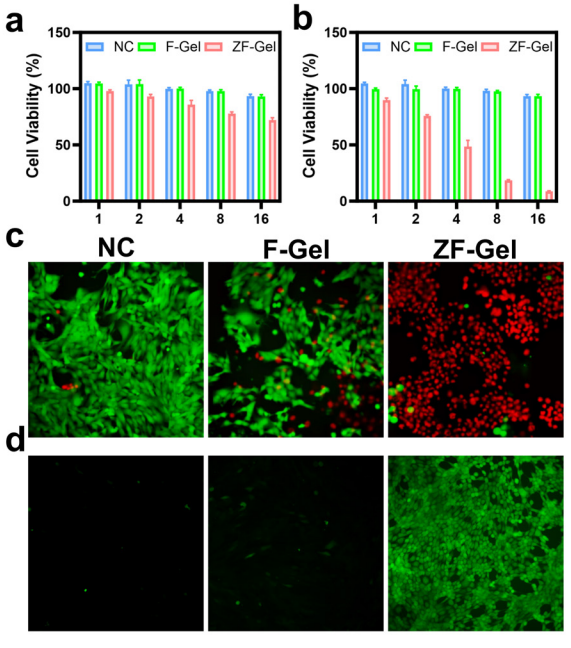

Figure 3. Biocompatibility, selective antitumor activity and ferroptosis induction of ZF-Gel. (a) Cell viability of HUVECs treated with F-Gel and ZF-Gel. (b) Cell viability of 4T1 cells treated with F-Gel and ZF-Gel. (c) Live/dead staining of 4T1 cells. (d) Lipid peroxidation fluorescence imaging in 4T1 cells.

Collectively, these results demonstrate that ZF-Gel selectively induces ferroptosis in 4T1 breast cancer cells

through robust oxidative stress and lipid peroxidation, while preserving the viability of normal endothelial cells. The favorable therapeutic window thus established underscores the translational potential of ZF-Gel as a safe and effective platform for intratumoral immunotherapy.

3.4 Activation of the cGAS-STING pathway

To elucidate the immunostimulatory mechanism underlying ZF-Gel-mediated antitumor activity, the activation status of the cGAS-STING signaling axis was evaluated by western blot analysis of IRF3 phosphorylation and quantitative RT-PCR quantification of downstream immune gene expression.

Western blot analysis (Fig. 4a) demonstrated marked upregulation of phosphorylated IRF3 (p-IRF3) in ZF-Gel-treated 4T1 cells relative to both the NC and F-Gel groups, whereas total IRF3 protein levels remained stable across all conditions, with β-actin confirming equal loading. The selective increase in p-IRF3 without a concomitant rise in total IRF3 indicates post-translational activation of the STING-TBK1-IRF3 axis, consistent with IRF3 phosphorylation and nuclear translocation rather than de novo transcriptional induction. This activation pattern is mechanistically attributable to cGAS-mediated sensing of cytosolic DNA liberated during ferroptosis-associated mitochondrial damage and nuclear envelope disruption, as well as Zn^{2+}-induced mitochondrial dysfunction and ROS-driven genomic DNA damage, collectively providing the upstream stimuli required for cGAS enzymatic activation and downstream STING engagement.

Quantitative RT-PCR analysis further corroborated these findings at the transcriptional level. GPX4 mRNA expression (Fig. 4b) was significantly downregulated in ZF-Gel-treated cells compared to the NC and F-Gel groups, which maintained comparable baseline transcript levels. As the central ferroptosis-suppressing enzyme, GPX4 neutralizes lipid hydroperoxides and constitutes the primary cellular defense against ferroptotic cell death. Transcriptional suppression of GPX4 in ZF-Gel-treated cells indicates that the system not only imposes exogenous oxidative stress via Fe^{3+}-catalyzed Fenton reactions, but concurrently dismantles endogenous antioxidant defenses at the transcriptional level. This dual vulnerability synergistically amplifies lipid peroxidation and lowers the ferroptosis threshold, an effect potentially attributable to Zn^{2+}-mediated disruption of mitochondrial membrane potential and consequent perturbation of redox-sensitive transcriptional regulators governing GPX4 expression.

Complementarily, IL-6 mRNA expression (Fig. 4c) was markedly upregulated in ZF-Gel-treated cells, whereas negligible levels were observed in the NC and F-Gel groups. As a pro-inflammatory cytokine regulated by IRF3 and NF-κB downstream of STING signaling, the elevated IL-6 expression further corroborates effective activation of the cGAS–STING pathway. This enhanced cytokine response indicates productive downstream transcriptional activity and suggests the establishment of a pro-inflammatory microenvironment conducive to immune cell recruitment and activation.

Collectively, these results demonstrate that ZF-Gel effectively activates the cGAS–STING–IRF3 signaling axis in 4T1 breast cancer cells, as evidenced by increased p-IRF3 expression, GPX4 downregulation, and marked IL-6 mRNA induction. This coordinated response suggests a mechanistic linkage between ferroptosis induction and innate immune activation. Specifically, Fe^{3+} and Zn^{2+} released from ZF NPs within the acidic tumor microenvironment promote lipid peroxidation-driven ferroptotic cell death while facilitating the generation of cytosolic DNA signals required for cGAS activation. Consequently, this process may convert immunologically silent tumor cell death into an immunostimulatory event, thereby bridging innate and adaptive antitumor immunity.

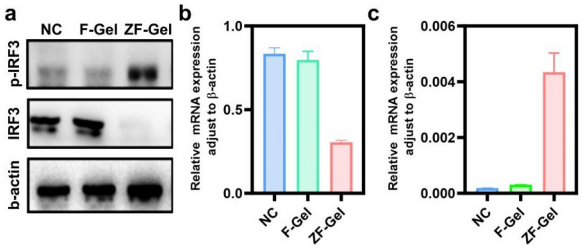

Figure 4. Activation of the cGAS-STING pathway by ZF-Gel. (a) Western blot analysis of p-IRF3 and total IRF3 in 4T1 cells. (b) Relative mRNA expression of GPX4. (c) Relative mRNA expression of IL-6.

4 Conclusion

In summary, we developed ZF-Gel, a Zn–Fe bimetallic MOF-integrated F127 thermosensitive hydrogel, as an injectable intratumoral platform for breast cancer immunotherapy. ZF NPs exhibited uniform morphology, well-defined crystallinity, and homogeneous elemental distribution, while ZF-Gel showed favorable mechanical stability, injectability, and effective intratumoral retention upon in situ gelation. *In vitro* results demonstrated that ZF-Gel selectively induced ferroptosis in 4T1 cells *via* Fe^{3+}-mediated Fenton reactions and Zn^{2+}-associated ROS amplification, as evidenced by enhanced lipid peroxidation and pronounced tumor cell death, with minimal cytotoxicity toward HUVECs. Mechanistically, ZF-Gel activated the cGAS-STING-IRF3 signaling axis, as indicated by increased p-IRF3 expression, GPX4 downregulation, and IL-6 upregulation, suggesting a functional coupling between ferroptosis and innate immune activation. Collectively, this work demonstrates that ZF-Gel integrates localized delivery, regulated ferroptosis, and immune pathway activation into a unified therapeutic strategy, providing a promising approach for remodeling the immunosuppressive microenvironment of immune-cold breast cancer. Future studies involving *in vivo* tumor models and systemic immune evaluation will be warranted to further validate its therapeutic efficacy and translational potential.

References

1. H. Sung, J. Ferlay, R.L. Siegel, M. Laversanne, I. Soerjomataram, A. Jemal, F. Bray, Global Cancer Statistics 2020: GLOBOCAN Estimates of Incidence and Mortality Worldwide for 36 Cancers in 185 Countries, CA: A Cancer Journal for Clinicians 71(3) (2021) 209-249.
2. L. Zhao, L. Jiang, L. He, Y. Wei, C. Jing, J. Li, et al., Targeting Ferroptosis in Cancer: From Mechanisms to Therapies, Cancer Communications 44(7) (2024) 755-772.
3. P. Schmid, J. Cortes, R. Dent, L. Pusztai, H. McArthur, S. Kümmel, et al., Event-free and Overall Survival According to Pathologic Complete Response in Patients with Early Triple-negative Breast Cancer, New England Journal of Medicine 386(6) (2022) 556-567
4. R. Demuynck, K.E. De Visser, M. Egeblad, Untangling the Web between Cytokines, Matrix Remodeling, and T Cell Suppression in the Tumor Microenvironment, Oncoimmunology 12(1) (2023) 2182632.
5. B.R. Stockwell, X. Jiang, W. Gu, Emerging Mechanisms and Disease Relevance of Ferroptosis, Trends in Cell Biology 30(6) (2020) 478-490.
6. I. Efimova, E. Catanzaro, L. Van der Meeren, V.D. Turubanova, H. Hammad, T.A. Mishchenko, et al., Vaccination with Early Ferroptotic Cancer Cells Induces Efficient Antitumor Immunity, Journal for ImmunoTherapy of Cancer 8(2) (2020) e001369.
7. X. Chen, R. Kang, G. Kroemer, D. Tang, Ferroptosis in Infection, Inflammation, and Immunity, Journal of Experimental Medicine 218(6) (2021) e20210518.
8. J. Lee, M.S. Kim, H.J. Kim, J.K. Ann, S.H. Goh, J.H. Lee, Iron-based Metal-organic Frameworks as Multifunctional Nanoplatforms for Combined Cancer Therapy, Coordination Chemistry Reviews 475 (2023) 214890.
9. A. Ablasser, Z.J. Chen, cGAS in Action: Expanding Roles in Immunity and Inflammation, Science 363(6431) (2019) eaat8657.
10. Z. Zhang, Z. Yao, L. Wang, H. Ding, J. Shao, A. Chen, et al., Activation of the cGAS-STING Signaling Pathway in Tumor-associated Macrophages Promotes Hepatocellular Carcinoma Metastasis, Cancer Communications 43(8) (2023) 879-903.
11. M. Li, Y. Shao, Y. Zhang, J. Zhang, P. Wu, Z. Chen, et al., Zinc Enhances cGAS-mediated Antitumor Immunity by Modulating STING Pathway Activation, Cancer Research Communications 3(5) (2023) 892-905.
12. J. Zhou, X. Du, J. Li, X. Du, J. Xu, C. Huang, et al., Metal-organic Frameworks for Drug Delivery and Cancer Therapy, Advanced Functional Materials 32(15) (2022) 2109785.
13. Y. Wu, Y. Zhang, D. Zhang, X. Jiang, G. Luo, M. Li, et al., Bimetallic Metal-organic Frameworks for Synergistic Cancer Immunotherapy via Ferroptosis and Immune Activation, ACS Nano 17(8) (2023) 7890-7905.
14. A. Sedykh, P. Pradeep, H. Zhu, H. Saigo, A.C. Kaushik, W. Wang, et al., Nanoparticle-mediated Drug Delivery and Tumor Retention: Challenges and Solutions, Drug Resistance Updates 63 (2022) 100837.
15. Y. Hu, Q. Zhang, Y. Gao, S. Li, L. Wang, J. Liu, et al., Thermosensitive Hydrogel for Localized and Sustained Delivery of Immunomodulatory Agents in Cancer Treatment, Biomaterials 293 (2023) 121947.